A Luminescent Heterometallic $Au^{I} \cdots Cu^{I}$ Complex. Spectroscopic Properties and Crystal Structures of $[Au(PPh_3)(C_7H_5N_2)]$ and $[\{Au(PPh_3)(\mu\text{-}C_7H_5N_2)Cu(\mu\text{-}C_7H_5N_2)\}_2]$ ($C_7H_5N_2$ = 7-azaindolate)†

Chi-Keung Chan, Chun-Xiao Guo, Kung-Kai Cheung, Dan Li and Chi-Ming Che*
Department of Chemistry, The University of Hong Kong, Pokfulam Road, Hong Kong

The mono- and tetra-nuclear complexes $[Au(PPh_3)(C_7H_5N_2)]$ **1** and $[\{Au(PPh_3)(\mu\text{-}C_7H_5N_2)Cu(\mu\text{-}C_7H_5N_2)\}_2]$ **2**, the latter containing 7-azaindolate ($C_7H_5N_2^-$) bridging ligands, have been prepared and their crystal structures determined. The intramolecular $Au \cdots Cu$ and $Cu \cdots Cu$ separations in **2** are 3.0104(6) and 2.941(1) Å respectively. Extended-Hückel molecular-orbital calculations revealed a weak $Au^{I} \cdots Cu^{I}$ bonding interaction but no $Cu^{I} \cdots Cu^{I}$ interaction. In acetonitrile, both complexes display intense intraligand emission at 510 nm upon photoexcitation with UV/VIS light at room temperature. In the solid state **2** shows an emission at 550 nm.

Studies on the spectroscopic and photochemical properties of luminescent dinuclear and polynuclear metal complexes have received much attention in recent years.[1-3] Previous studies by Balch and co-workers[4] revealed quite a number of interesting luminescent mixed-metal complexes, which incorporate both Ir^{I} and Au^{I}. Our recent studies on the complexes $[Pt^{II}Rh^{I}(dppm)_2(CN)_2(CNBu^{t})_2]^{+}$[5] and $[Pt^{II}Au^{I}(dppm)_2(CN)_2]^{+}$[6] [dppm = bis(diphenylphosphino)methane] are also in line with these results suggesting that heterobimetallic complexes having weak intramolecular metal–metal interactions comprise a new class of photoluminescent materials with potential photochemical properties. Owing to the substantial number of Au^{I}[3,7] and Cu^{I}[2] clusters which are known to be emissive in solution at room temperature, heterometallic complexes with $Au^{I} \cdots Cu^{I}$ interactions are of interest.

Heterometallic complexes comprising both Au^{I} and Cu^{I} are not unknown; Knobler and co-workers[8] reported the synthesis and crystal structure of $[Au_3Cu_2(C{\equiv}CPh)_6]^{-}$ with Au^{I}–Cu^{I} distances in the range 2.783–3.016(3) Å, and Vicente and co-workers[9] recently found that the tendency of d^{10} coinage-metal ions to form aggregates easily led to the formation of a whole range of heterometallic d^{10} clusters. In this contribution, the synthesis, electronic structure and spectroscopic properties of a tetranuclear metal complex having a Au_2Cu_2 core is described.

Experimental

Materials.—Silver trifluoromethanesulfonate and 7-azaindole (1*H*-pyrrolo[2,3-*b*]pyridine) were purchased from Aldrich. Triethylamine (from Merck) was dried over KOH before use. The complexes $[Au(PPh_3)Cl]$[10] and $[CuCl(PPh_3)_3]$[11] were prepared by literature methods. All solvents for syntheses were analytical grade, whilst those for emission studies and lifetime measurements were purified according to the methods reported by Perrin and Armarego.[12]

Syntheses.—$[Au(PPh_3)(C_7H_5N_2)]$ **1**. A suspension of $[Au(PPh_3)Cl]$ (100 mg, 0.2 mmol) in methanol (20 cm^3) was stirred with 7-azaindole (24 mg, 0.2 mmol) in the presence of triethylamine (0.05 cm^3) until the solution became clear and colourless (*ca.* 30 min). Addition of $AgCF_3SO_3$ (51 mg, 0.2 mmol) to the solution gave a precipitate of AgCl which was filtered off and the filtrate was reduced to ≈5 cm^3; colourless crystals were obtained by vapour diffusion of diethyl ether into this solution. Yield 80%. NMR($CDCl_3$): ^1H, δ 6.46–6.47 (d, 1 H, J = 2.93, pyrrolic-β H), 6.90–6.94 (q, 1 H, J = 2.93, pyrrolic-α H), 7.43–7.64 (m, 15 H, Ph), 7.66 (d, 1 H, J = 1.47, pyridyl-γ H), 7.93–7.96 (dd, 1 H, J = 1.47, pyridyl-β H), 8.24–8.26 (dd, 1 H, J = 1.47 Hz, pyridyl-α H); ^{31}P-{^1H}, δ 32.6.

$[\{Au(PPh_3)(\mu\text{-}C_7H_5N_2)Cu(\mu\text{-}C_7H_5N_2)\}_2]$ **2**. A suspension of **1** (69 mg, 0.12 mmol) and $[CuCl(PPh_3)_3]$ (105 mg, 0.12 mmol) in CH_2Cl_2 (20 cm^3) was stirred at room temperature for 30 min. A yellow solution was obtained, which was filtered over Celite and the filtrate concentrated down to 5 cm^3. Addition of diethyl ether gave a yellow solid, with yellow crystals being obtained by vapour diffusion of diethyl ether into a dichloromethane solution. Yield 50%. NMR(CD_2Cl_2): ^1H, δ 6.44–6.47 (m, 4 H, pyrrolic-β H), 6.88–6.90 (m, 4 H, pyrollic-α H), 7.44–7.62 (m, 30 H, Ph), 7.93–8.11 (m, 12 H, pyridyl H); ^{31}P-{^1H}, δ 31.6.

Physical Measurements and Instrumentation.—Proton and ^{31}P NMR were recorded on a JEOL 270 multinuclear FT-NMR spectrometer. Chemical shifts (δ, ppm) were reported relative to tetramethylsilane (^1H) and external H_3PO_4 (^{31}P). The UV/VIS spectra were recorded on a Milton Roy Spectronic 3000 array spectrometer and steady-state emission spectra on a SPEX Fluorolog-2 spectrofluorometer. Emission-lifetime measurements were performed with a Quanta Ray DCR-3 Nd-YAG laser (pulsed output 355 nm, 8 ns). The decay signal was recorded using a R928 PMT (Hamamatsu) digitized with a Tektronix 2430 digital oscilloscope interfaced to an IBM PC/AT computer, equipped with single exponential fitting. Solutions for photochemical experiments were degassed by at least four freeze–pump–thaw cycles.

Molecular-orbital Calculations.—Extended-Hückel molecular-orbital (EHMO) calculations were carried out using the geometric parameters from the X-ray diffraction data. The basis functions of Au and Cu contain their corresponding s, p and d orbitals. All the parameters and calculations involved were made with the Argus program.[13]

† *Supplementary data available:* see Instructions for Authors, *J. Chem. Soc., Dalton Trans.*, 1994, Issue 1, pp. xxiii–xxviii.

Table 1 Crystallographic data for compounds **1** and **2**

	1	**2**
Formula	$C_{25}H_{20}AuN_2P$	$C_{64}H_{50}Au_2Cu_2N_8P_2$
M	576.39	1514.12
Crystal system	Monoclinic	Triclinic
Space group	$P2_1/n$	$P\bar{1}$
a/Å	9.145(1)	11.204(1)
b/Å	18.258(2)	11.376(1)
c/Å	13.470(2)	12.727(2)
α/°	90	115.62(1)
β/°	108.93(1)	106.31(1)
γ/°	90	93.05(1)
U/Å^3	2139(1)	1375.0(1.0)
D/g cm^3	1.790	1.828
Z	4	2
μ/cm^{-1}	69.50	61.81
R	0.025	0.029
R'	0.031	0.036
$F(000)$	1112	736
Goodness of fit, S	1.07	1.261

Table 2 Atomic coordinates of non-hydrogen atoms with estimated standard deviations (e.s.d.s) in parentheses for complex **1**

Atom	x	y	z
Au	0.172 29(2)	0.109 47(1)	0.121 58(1)
P	0.129 7(1)	0.014 75(6)	0.213 33(8)
N(1)	0.216 6(4)	0.198 9(2)	0.046 1(3)
N(2)	0.480 5(4)	0.210 3(2)	0.149 5(3)
C(1)	0.215 5(4)	0.030 0(2)	0.352 4(3)
C(2)	0.165 7(5)	−0.005 8(3)	0.427 4(3)
C(3)	0.239 6(5)	0.004 5(3)	0.532 3(4)
C(4)	0.362 1(5)	0.052 0(3)	0.566 0(4)
C(5)	0.412 0(5)	0.089 4(3)	0.494 0(4)
C(6)	0.339 2(5)	0.078 7(3)	0.387 0(4)
C(7)	0.205 9(4)	−0.071 6(2)	0.185 6(3)
C(8)	0.251 9(6)	−0.127 0(3)	0.260 0(4)
C(9)	0.311 0(6)	−0.192 1(3)	0.235 7(4)
C(10)	0.323 4(6)	−0.202 4(3)	0.138 1(4)
C(11)	0.277 3(6)	−0.148 0(3)	0.063 6(4)
C(12)	0.219 1(5)	−0.082 9(3)	0.087 9(4)
C(13)	−0.072 2(4)	−0.001 3(3)	0.192 5(3)
C(14)	−0.141 0(5)	−0.068 3(3)	0.165 7(4)
C(15)	−0.297 9(5)	−0.076 6(4)	0.144 2(5)
C(16)	−0.386 4(6)	−0.017 7(4)	0.150 6(4)
C(17)	−0.320 4(5)	0.048 9(3)	0.179 7(4)
C(18)	−0.163 4(5)	0.058 2(3)	0.199 3(4)
C(19)	0.122 0(7)	0.235 9(3)	−0.038 3(4)
C(20)	0.200 2(7)	0.290 7(3)	−0.069 3(4)
C(21)	0.352 3(5)	0.288 6(3)	−0.000 9(4)
C(22)	0.489 1(6)	0.326 2(3)	0.012 9(4)
C(23)	0.615 7(7)	0.305 9(4)	0.093 1(5)
C(24)	0.608 5(7)	0.248 8(3)	0.161 0(5)
C(25)	0.358 4(5)	0.230 3(3)	0.070 9(3)

Table 3 Atomic coordinates of non-hydrogen atoms with e.s.d.s in parentheses for complex **2**

Atom	x	y	z
Au	0.016 46(2)	0.398 86(2)	0.140 99(2)
Cu	−0.073 49(5)	0.101 55(5)	−0.006 08(5)
P	0.206 6(1)	0.422 8(1)	0.274 7(1)
N(1)	−0.156 1(4)	0.404 2(4)	0.036 8(4)
N(2)	−0.257 3(4)	0.174 1(4)	−0.071 7(3)
N(3)	0.094 1(4)	−0.104 6(3)	−0.138 6(3)
N(4)	−0.012 8(4)	0.071 2(3)	−0.140 1(3)
C(1)	−0.199 6(5)	0.519 2(5)	0.048 2(5)
C(2)	−0.324 7(5)	0.493 7(5)	−0.016 8(5)
C(3)	−0.367 3(5)	0.354 6(5)	−0.074 5(4)
C(4)	−0.480 1(5)	0.261 4(6)	−0.151 3(5)
C(5)	−0.480 4(5)	0.130 5(6)	−0.185 8(5)
C(6)	−0.368 8(5)	0.090 8(5)	−0.146 5(5)
C(7)	−0.259 5(5)	0.302 9(4)	−0.037 5(4)
C(8)	0.161 6(5)	−0.183 7(5)	−0.204 0(4)
C(9)	0.178 8(6)	−0.164 9(7)	−0.298 7(6)
C(10)	0.098 9(8)	−0.040 0(7)	−0.288 0(5)
C(11)	0.080(1)	0.023(1)	−0.333(1)
C(12)	0.011 0(7)	0.116 8(7)	−0.296 8(6)
C(13)	−0.034 0(5)	0.143 0(5)	−0.202 7(4)
C(14)	0.056 2(5)	−0.021 5(4)	−0.184 2(4)
C(15)	0.280 9(4)	0.597 0(4)	0.367 5(4)
C(16)	0.364 1(5)	0.648 7(5)	0.488 4(4)
C(17)	0.420 0(6)	0.780 7(6)	0.555 1(5)
C(18)	0.399 1(6)	0.864 2(5)	0.501 8(5)
C(19)	0.319 7(6)	0.812 5(5)	0.381 7(5)
C(20)	0.259 5(5)	0.681 4(5)	0.315 8(4)
C(21)	0.322 4(4)	0.345 1(4)	0.206 8(4)
C(22)	0.282 2(5)	0.223 9(5)	0.102 3(5)
C(23)	0.368 2(6)	0.163 1(6)	0.048 6(5)
C(24)	0.494 3(5)	0.222 1(6)	0.099 2(5)
C(25)	0.534 9(5)	0.343 8(6)	0.203 8(5)
C(26)	0.449 7(5)	0.406 8(5)	0.256 9(4)
C(27)	0.200 5(4)	0.365 7(4)	0.387 3(4)
C(28)	0.144 6(6)	0.431 6(6)	0.472 7(5)
C(29)	0.145 4(7)	0.390 0(8)	0.562 9(5)
C(30)	0.198 3(7)	0.287 2(6)	0.564 8(6)
C(31)	0.251 5(8)	0.223 7(7)	0.479 2(6)
C(32)	0.253 1(7)	0.261 7(6)	0.389 8(5)

Crystal-structure Determinations.—Single crystals of **1** and **2** were obtained by vapour diffusion of diethyl ether into dichloromethane solution at room temperature, dimensions 0.07 × 0.20 × 0.25 for **1** and 0.10 × 0.15 × 0.20 mm for **2**. All diffraction data were collected with graphite-monochromated Mo-Kα radiation (λ = 0.7107 Å) on an Enraf-Nonius CAD-4 diffractometer at 24 °C, using the ω–2θ scan mode up to $2\theta_{max}$ = 56.0° for **1** and 52.0° for **2**. An empirical-absorption correction was applied on the basis of the ψ scan of the 7 strongest reflections for **1** and 5 for **2**. For **1** (**2**), 5158 (5377) independent reflections were measured, 3325 (4467) of which those with $F_o > 6.0\sigma(F_o)$ were used in structural refinement. All the diffraction data were corrected for Lorentz and polarization effects.

The structures were solved by Patterson and Fourier methods and refined by full-matrix least squares with atomic scattering factors from ref. 14 using the Enraf-Nonius SDP-1985 programs[15] on a MicroVAX II computer. Non-hydrogen atoms were refined anisotropically. Convergence by least-squares refinement on F_o with $w = 4F_o^2/\sigma^2(F_o^2)$ where $\sigma^2(F_o) = [\sigma^2(I) + (0.04F_o^2)^2]$ for reflections with $I \geqslant 3.0\sigma(I)$. Variables were involved in the refinement: 262 for **1** and 352 for **2**. Hydrogen atoms were located in a difference map but not refined. The final Fourier-difference maps for both **1** and **2** were featureless, with respective maximum positive and negative peaks of 0.63 and 0.49 for **1** and 0.68 and 0.68 e Å^{-3} for **2**. A summary of the crystal data are given in Table 1, and atomic coordinates for **1** and **2** are in Tables 2 and 3 respectively.

Additional material available from the Cambridge Crystallographic Data Centre comprises H-atom coordinates, thermal parameters and remaining bond lengths and angles.

Results and Discussion

Syntheses and Crystal Structures.—The use of 7-azaindole as a bridging ligand for the synthesis of face-to-face dinuclear metal complexes has been reported in several cases.[16] Recent studies also showed that this ligand reacts with divalent metal ions to give tetranuclear $[M_4O(C_7H_5N_2)_6]$ complexes,[16,17] the Zn^{II} derivative of which has been found to display interesting emission properties.[17b]

Our attempt to prepare a dinuclear gold(I) complex by treating $[Au(PPh_3)Cl]$ with 7-azaindole led to the isolation of $[Au(PPh_3)(C_7H_5N_2)]$ **1**. Presumably, the ligand bite distance of

7-azaindole which is estimated to be 2.38 Å, is too short for two Au^{I} to be held together. Complex **1** is an air-stable solid with low solubility in acetonitrile and dichloromethane.

Fig. 1 shows an ORTEP drawing of **1**.[18] The Au^{I} is two-co-ordinated by a phosphorus and a nitrogen atom, the latter being the deprotonated pyrrolic nitrogen of 7-azaindolate instead of the pyridyl group. The P–Au–N angle of 176.6(2)° is similar to the related value of 176.0(5)° found in $[AuCl(NC_5H_{11})]$[19] (NC_5H_{11} = piperidine), and the Au–N(amide) distance of 2.033(5) Å is comparable to those in $[N(AuPPh_3)_5]^{2+}$ [1.99(1)–2.04(1) Å][20] and $[(AuPPh_3)_3(NC_6H_{11})]^{+}$ [2.040(5)–2.059(5) Å].[21]

The pendant pyridyl group in **1** is essential to the generation of the heterobimetallic complex as it can co-ordinate further metal ions. Complex **2** was prepared by treating **1** with $[CuCl(PPh_3)_3]$; $[Au(PPh_3)Cl]$ was also obtained as a side product. A tentative reaction scheme is suggested in Scheme 1. It is quite likely that the weak $Au^{I} \cdots Cu^{I}$ interaction provides the driving force for the formation of **2**.

An ORTEP drawing showing the perspective view of the structure of **2** is depicted in Fig. 2. The molecule has a crystallographically imposed C_{2h} symmetry about the Cu–Cu′ vector. The Cu and Au atoms are best described as lying at the vertices of a parallelogram, with sides of length 3.0104(6) and 5.3213(6) Å corresponding to the Au–Cu and Au–Cu′ distances respectively, with Au–Cu–Cu′ 26.81(2)°. As in **1**, each Au^{I} co-ordinates to PPh_3 and the pyrrolic nitrogen atom of 7-azaindolate in a nearly linear configuration. The P–Au–N angle of 171.8(1)° is slightly smaller than the related value of 176.6(2)° found in **1**. This may be due to the weak $Au^{I} \cdots Cu^{I}$ bonding interaction, which causes slight bending of the P–Au–N axis. The intramolecular $Au^{I} \cdots Cu^{I}$ separation of 3.0104(6) Å falls within the range of 2.783–3.016(3) Å found in $[NBu^{n}_4][Au_3Cu_2(C{\equiv}CPh)_6]$.[8a] The results of molecular orbital calculations (see below) imply that there is a weak $Au^{I} \cdots Cu^{I}$ bonding interaction of similar distance. The co-ordination geometry about each Cu^{I} is a distorted T shape [N–Cu–N 98.5(2), 98.7(2) and 162.6(2)°] and the intramolecular $Cu \cdots Cu'$ separation is 2.941(1) Å, which is longer than twice the van der Waal's radius of Cu [2.80 Å]. Even though this separation is shorter than that of $Au^{I} \cdots Cu^{I}$ EHMO calculations do not reveal the existence of a $Cu^{I} \cdots Cu^{I}$ bonding interaction.

Extended-Hückel Molecular-orbital Calculations.—An EHMO calculation has been performed on **2**, and the molecular-orbital diagram is shown in Fig. 3. Most of the orbitals can be considered as single bonding. Both the HOMO (highest-occupied MO) and the next highest occupied orbital consist of the d_{z^2} orbital of copper (69% and 55% respectively) and the p_z orbitals of 7-azaindolate (18% and 24% respectively). The remaining d orbitals of Cu are considerably lower in energy and lie in the range −10.5 to −10.75 eV. The two lowest unoccupied

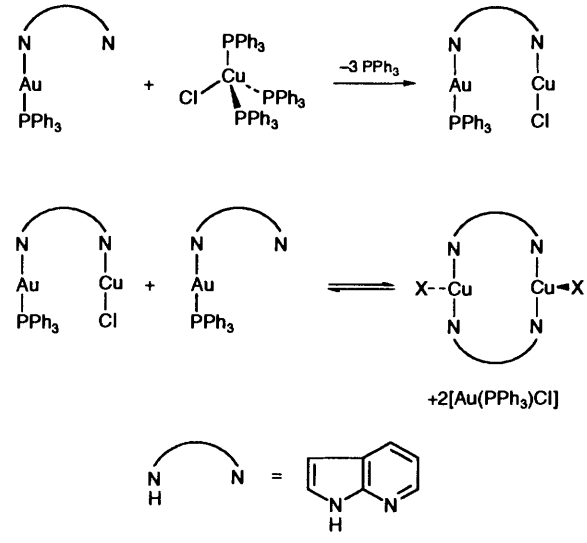

Scheme 1 Suggested reaction pathway for the tetrameric Au_2Cu_2 system; X = $[Au(PPh_3)(C_7H_5N_2)]$

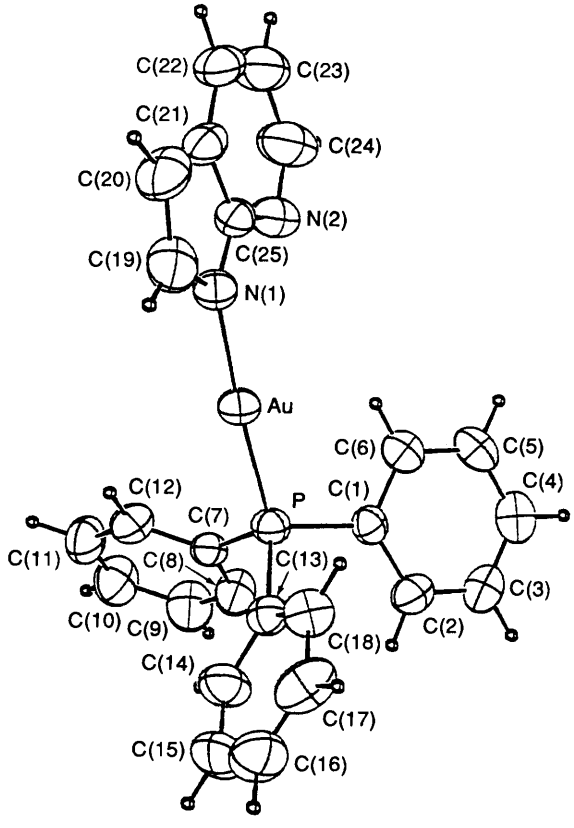

Fig. 1 An ORTEP drawing of **1** with numbering. Selected bond distances (Å) and bond angles (°): Au–P 2.233(1), Au–N(1) 2.033(5); P–Au–N(1) 176.6(2)

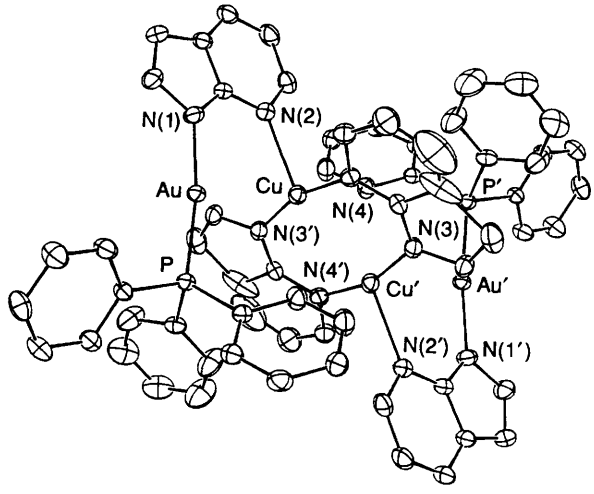

Fig. 2 An ORTEP drawing of **2** with atom numbering, H atoms omitted for clarity. Selected bond distances (Å) and bond angles (°): Au–P 2.239(1), Au–N(1) 2.035(5), $Au \cdots Cu$ 3.0104(6), Cu–N(2) 2.330(5), Cu–N(4) 1.912(4), Cu–N(3) 1.905(5), $Cu \cdots Cu'$ 2.941(1), $Au \cdots Cu'$ 5.3213(6); N(1)–Au–P 171.8(1), N(2)–Cu–N(4) 98.7(2), N(4)–Cu–N(3) 162.6(2), N(2)–Cu–N(3) 98.5(2), Au–Cu–N(3) 87.5(1), Au–Cu–Cu′ 126.81(2). Symmetry operation(′): $-x, -y, -z$.

Table 4 Calculated molecular-orbital energies and charge distribution for compound **2**

		Charge distribution (%)									
Molecular orbital	Energy/eV	Au/Au'	Cu/Cu'	L_1	L_2	P	3Ph	L_3	L_4	P'	3Ph'
π* (phenyl rings)	−6.8885	0.16	0.12	0.05	1.56	0.00	48.24	0.05	1.56	0.00	48.25
π* (L_2, L_4)	−7.1239	0.28	0.55	0.03	45.64	0.03	3.38	0.03	45.64	0.03	3.88
π* (L_2, L_4)	−7.1500	0.45	0.59	0.11	46.76	0.12	2.49	0.11	46.76	0.12	2.49
π* (L_1, L_3)	−7.8069	0.03	0.08	49.74	0.08	0.00	0.12	49.74	0.08	0.00	0.12
π* (L_1, L_3)	−7.8096	0.03	0.13	49.72	0.06	0.00	0.15	49.72	0.06	0.00	0.15
ψ_1[Cu(d_{z^2}) + N(p_z)]	−9.8024	4.89	69.31	3.29	6.01	1.82	1.79	3.29	6.01	1.82	1.79
ψ_2[Cu(d_{z^2}) + N(p_z)]	−9.9270	7.10	54.69	2.44	9.89	3.11	3.66	2.44	9.89	3.11	3.66
d_{σ}*(Au–Cu)	−10.2526	19.30	16.60	2.68	1.18	13.32	14.87	2.68	1.18	13.32	14.87
d_{σ}*(Au–Cu)	−10.2712	16.05	23.08	3.50	1.84	11.76	13.34	3.50	1.84	11.76	13.34
Cu d block[a]	−10.5128	0.10	79.93	0.22	9.49	0.10	0.17	0.22	9.49	0.10	0.17
Cu d block[a]	−10.5504	0.02	95.10	0.17	2.26	0.00	0.01	0.17	2.26	0.00	0.01
Cu d block[a]	−10.6024	0.04	93.61	0.05	3.12	0.00	0.01	0.05	3.12	0.00	0.01

[a] Excluding d_{z^2}.

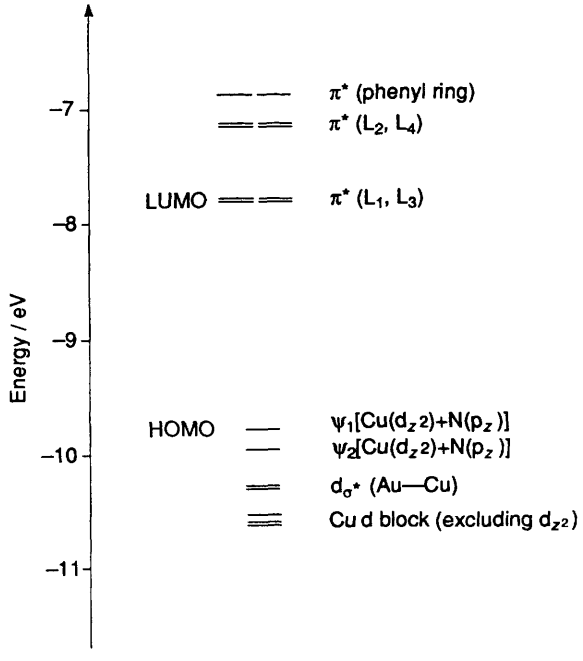

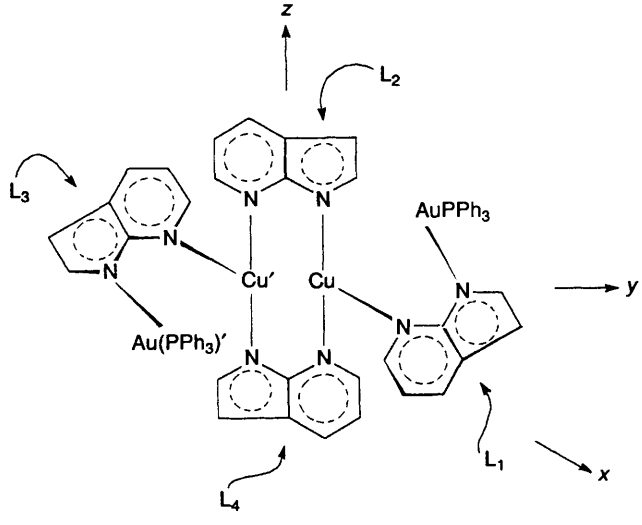

Fig. 3 Molecular-orbital diagram of **2**

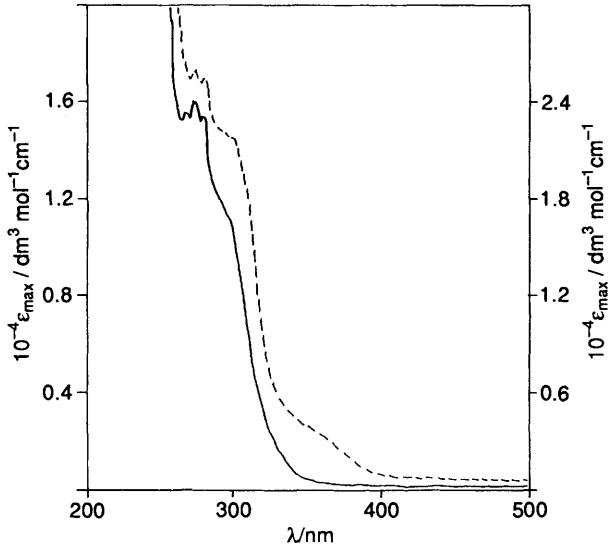

Fig. 4 The UV/VIS absorption spectra of **1** (——) and **2** (– – – –) in acetonitrile at room temperature

MOs (LUMOs) at −7.8069 and −7.8096 eV mainly comprise the π* orbitals of 7-azaindolate. A summary of the combination of the atomic orbitals in the resultant molecular orbitals is given in Table 4.

Although the charge density of Cu (0.94e) is greater than that of Au (0.74e) both are approximately +1e. The Milliken bond order for the $Au^{I} \cdots Cu^{I}$ interaction is 0.033. The electronic configurations of Cu and Au are $[Ar]3d^{9.93}4s^{0.32}4p^{-0.19}$ and $[Xe]5d^{9.86}6s^{0.61}6p^{-0.21}$ respectively, suggesting that the interaction between these centres involves the 4s(Cu), 4p(Cu) and 6s(Au) orbitals. There is no interaction between the two Cu^{I} atoms as the Milliken bond order between them was found to be zero. The charge densities of the azaindolate ligands are in the range −0.93 to −0.95e, which is consistent with an electronic charge on the pyrrolic nitrogen.

Photophysical Properties of the Complexes.—The UV/VIS absorption spectra of **1** and **2** shown in Fig. 4 are featureless. Complex **1** displays an intense high energy absorption at 269 nm ($\varepsilon_{max} = 1.55 \times 10^4$ dm^3 mol^{-1} cm^{-1}) and a shoulder at 294 nm. These are assigned to the intraligand $^1(\pi_2) \longrightarrow {}^1(\pi,\pi^*)$ transition of 7-azaindolate since a similar absorption band is also found in unbound 7-azaindole ($\varepsilon_{max}^{269} = 7.28 \times 10^3$ dm^3 mol^{-1} cm^{-1}). There are also weaker absorptions from 300

Table 5 Photophysical data for 1*H*-pyrrolo[2,3-*b*]pyridine and complexes **1** and **2**

Compound	Medium (*T*/K)	λ/nm (τ_0/μs)	$10^2\ \varphi^{em}$
$C_7H_6N_2$	MeCN (298)	358 (< 10 ns)	0.25
1	MeCN (298)	390 (< 10 ns), 520 (6.1)	0.48
	EtOH–MeOH glass (77)	450, 470, 500, 520	
2	MeCN (298)	440 (< 10 ns), 510 (1.9)	0.1
	CH_2Cl_2 (298)	440 (< 10 ns)	0.44
	solid (77)	550 (3.5)	

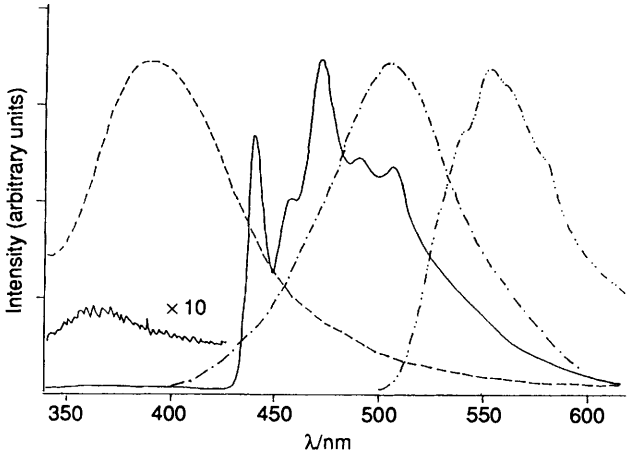

Fig. 5 Emission spectrum of **1** in EtOH–MeOH (v/v 4:1) solution at room temperature (– – –) and glass (——) at 77 K, and **2** in CH_3CN (—·—·—) at room temperature and in the solid state (—··—··—) at 77 K

to 350 nm. Complex **2** shows a broad absorption ranging from 250 to 400 nm. As in **1**, the high energy absorptions at 269 and 294 nm ($\varepsilon_{max}^{269} = 2.66 \times 10^3$ dm^3 mol^{-3} cm^{-1}) are assigned to the 7-azaindolate intraligand transition. The broad absorption band centred at 365 nm deserves some attention. It is well known that for some polynuclear Au^I complexes,[3a,b] intramolecular Au^I–Au^I interaction leads to the stabilization of the p_σ and destabilization of the d_{σ^*} orbitals [here p_σ and d_{σ^*} refer to the σ-bonding combination of the $(n + 1)$p orbitals and the σ-antibonding combination of the *n*d orbitals of the metal ions respectively]. This gives rise to a relatively lower energy $d_{\sigma^*} \longrightarrow p_\sigma$ transition, which is dipole-allowed and is absent in the absorption spectrum of the corresponding mononuclear Au^I complexes.[22] Here, the HOMO and LUMO of **2** as revealed by molecular-orbital calculation are the d_{z^2} orbital of Cu^I and the π* of 7-azaindolate respectively. Accordingly, the low energy absorption of **2** at 365 nm is likely to be [Cu ⟶ π*($C_7H_5N_2$)] in nature.

Photoluminescence has been observed from free 7-azaindole and from complexes **1** and **2**, and the data are summarized in Table 5. At room temperature and upon excitation at 290 nm in acetonitrile, the free 7-azaindole displays an intense fluorescence at 358 nm, while the intraligand phosphorescence is too weak to be recorded. The ligand emission, nonetheless, is strongly affected by Au^I. Fig. 5 depicts the emission spectrum of **1** measured in EtOH–MeOH (v/v 4:1) at room temperature and at 77 K, showing an intense emission band at 390 nm and a shoulder at around 500 nm, which are assigned to intraligand fluorescence and phosphorescence respectively. Cooling to 77 K results in the enhancement of the intraligand phosphorescence, which becomes vibronically well-resolved. The enhancement of the intraligand phosphorescence through co-ordination to Au^I has been observed in several cases.[3d,23]

The emission spectrum of **2** in degassed acetonitrile is also shown in Fig. 5, and is quite similar to that of **1**. However in the solid state the spectrum is quite different, and the emission maximum is red shifted to 550 nm with a lifetime of *ca.* 3.5 μs. Such a low energy emission is unlikely to be due to intraligand phosphorescence, and could be either a metal-centred transition or due to metal-to-ligand charge transfer (m.l.c.t.).

Conclusion

In certain homodinuclear Pt^{II}–Pt^{II} [1d,24] and polynuclear Au^I–Au^I [3,7a,b] complexes the occurrence of a relatively low energy intense absorption band is taken to indicate the existence of weak intramolecular metal–metal interactions and has been assigned to the $d_{\sigma^*} \longrightarrow p_\sigma$ transition. In the heterobimetallic Pt^{II}–Rh^I [15] and Pt^{II}–Au^I [16] complexes studied before, such low energy absorption bands also exist although they are not quite the same as the $d_{\sigma^*} \longrightarrow p_\sigma$ transitions of homobimetallic complexes. Here, the objective was to study the interaction between Au^I and Cu^I by spectroscopic means. Although some interaction between these two metals in complex **2** is inferred by both the results of EHMO calculations and to some extent by the observed $Au^I \cdots Cu^I$ distance of 3.0104(6) Å, we could not locate any electronic absorption band similar to that of the $d_{\sigma^*} \longrightarrow p_\sigma$ transition in $[Au_2(dppm)_2]^{2+}$ [3a] in the UV/VIS absorption spectrum.

The EHMO calculations reveal that the lowest energy dipole-allowed transition in **2** is likely to be m.l.c.t. [Cu ⟶ π*($C_7H_5N_2$)] in nature. However, while the $Au^I \cdots Cu^I$ interaction may exist in the solid state, it may not exist in solution owing to the non-rigid structure of the complex; this is confirmed by the difference in emission properties in the solid state and in solution. Previous studies showed that weak metal–metal interactions in polynuclear Au^I complexes give rise to a visible emission.[3] Thus for the complex $[\{Au_2(dppe)(C{\equiv}CPh)_2\}_2]$ [23] [dppe = bis(diphenylphosphino)ethane], a solid-state emission at 550 nm was observed whereas only the intraligand phosphorescence of the co-ordinated phenylacetylide was recorded in acetonitrile. This has been attributed to the intermolecular $Au^I \cdots Au^I$ interaction in the solid form disappearing in solution, and in this context, complex **2** resembles $[\{Au_2(dppe)(C{\equiv}CPh)_2\}_2]$. The solution emission spectrum of **2** is dominated by the intraligand phosphorescence of 7-azaindolate whereas in the solid state a visible emission is observed.

Acknowledgements

We acknowledge support from the University of Hong Kong and the Research Grants Council.

References

1 (*a*) H. B. Gray and A. W. Maverick, *Science*, 1981, **214**, 1201; (*b*) D. G. Nocera, A. W. Maverick, J. R. Winkler, C.-M. Che and H. B. Gray, *ACS Symp. Ser.*, 1983, **211**, 20; (*c*) D. C. Smith and H. B. Gray, *Coor. Chem. Rev.*, 1990, **100**, 169; (*d*) D. M. Roundhill, H. B. Gray and C.-M. Che, *Acc. Chem. Res.*, 1989, **22**, 55; (*e*) J. K. Nagle, A. L. Balch and M. M. Olmstead, *J. Am. Chem. Soc.*, 1988, **110**, 319.

2 P. C. Ford and A. Vogler, *Acc. Chem. Res.*, 1993, **26**, 220 and refs. therein.
3 (*a*) C.-M. Che, H. L. Kwong, C.-K. Poon and V. W.-W. Yam, *J. Chem. Soc., Dalton Trans.*, 1990, 3215; (*b*) C.-M. Che, H.-K. Yip, V. W.-W. Yam, P.-Y. Cheung, T.-F. Lai, S.-J. Shieh and S.-M. Peng, *J. Chem. Soc., Dalton Trans.*, 1992, 427; (*c*) D. Li, C.-M. Che, S.-M. Peng, S.-T. Liu, Z.-Y. Zhou and T. C.-W. Mak, *J. Chem. Soc., Dalton Trans.*, 1993, 189; (*d*) B.-C. Tzeng, D. Li, S.-M. Peng and C.-M. Che, *J. Chem. Soc., Dalton Trans.*, 1993, 2365.
4 See, for example, A. L. Balch, V. J. Catalano, B. C. Noll and M. M. Olmstead, *J. Am. Chem. Soc.*, 1990, **112**, 7558; A. L. Balch and V. J. Catalano, *Inorg. Chem.*, 1991, **30**, 1302; A. L. Balch and V. J. Catalano, *Inorg. Chem.*, 1992, **31**, 3934; A. L. Balch and V. J. Catalano, *Inorg. Chem.*, 1992, **31**, 2569.
5 H.-K. Yip, H.-M. Liu, Y. Wang and C.-M. Che, *Inorg. Chem.*, 1993, **32**, 3402.
6 H.-K. Yip, C.-M, Che and S.-M. Peng, *J. Chem. Soc., Chem. Commun.*, 1991, 1626; H.-K. Yip, H.-M. Lin, K.-K. Cheung, C.-M. Che and Y. Wang, *Inorg. Chem.*, 1994, **33**, 1644.
7 (*a*) S. Wang, G. Garz'en, C. King, J.-C. Wang and J. P. Fackler, jun., *Inorg. Chem.*, 1989, **28**, 4623; (*b*) C. King, M. N. I. Khan, R. J. Staples and J. P. Fackler, jun., *Inorg. Chem.*, 1992, **31**, 3236; (*c*) T. M. McCleskey and H. B. Gray, *Inorg. Chem.*, 1992, **31**, 1733.
8 (*a*) O. M. Abu-Salah, A.-R. A. Al-Ohaly and C. B. Knobler, *J. Chem. Soc., Chem. Commun.*, 1985, 1502; (*b*) O.-M. Abu-Salah and C. B. Knobler, *J. Organomet. Chem.*, 1986, **302**, C10.
9 J. Vicente, M.-T. Chicote and M.-C. Lagunas, *Inorg. Chem.*, 1993, **32**, 3748; J. Vicente, M.-T. Chicote, M.-C. Lagunas and P. G. Jones, *J. Chem. Soc., Chem. Commun.*, 1991, 1730.
10 M. I. Bruce, B. K. Nicholson and O. B. Shawkataly, *Inorg. Synth.*, 1989, **26**, 324.
11 F. H. Jardine, L. Rule and A. G. Vohra, *J. Chem. Soc. A*, 1970, 238.
12 D. D. Perrin, W. L. F. Armarego and D. R. Perrin, *Purification of Laboratory Chemicals*, Pergamon, 2nd edn., 1980, pp. 78–81.
13 M. A. Thompson, *A Quantum Chemical Electronic Structure Program Version 1.1 User Manual*, August, 1992.
14 *International Tables for X-ray Crystallography*, Kynoch Press, Birmingham, 1974, vol. 4.
15 Enraf-Nonius Structure Determination Package, Enraf-Nonius, Delft, 1985.
16 R. W. Brookes and R. L. Martin, *Inorg. Chem.*, 1975, **14**, 528.
17 (*a*) S.-M. Peng and Y.-N. Liu, *Acta. Crystallogr., Sect. C*, 1986, **42**, 1725; (*b*) C.-F. Lee, K. F. Chin, S.-M. Peng and C.-M. Che, *J. Chem. Soc., Dalton Trans.*, 1993, 467.
18 C. K. Johnson, ORTEP II, Report ORNL-5138, Oak Ridge National Laboratory, Oak Ridge, TN, 1976.
19 J. J. Guy, P. G. Jones, M. J. Mays and G. M. Sheldrick, *J. Chem. Soc., Dalton Trans.*, 1977, 8.
20 E. Zeller, H. Beruda, A. Kolb, P. Bissinger, J. Riede and H. Schmidbaur, *Nature (London)*, 1991, **352**, 141; A. Grohmann, J. Riede and H. Schmidbaur, *Nature (London)*, 1990, **345**, 140.
21 H. Schmidbaur, A. Kolb and P. Bissinger, *Inorg. Chem.*, 1992, **31**, 4370.
22 H. R. C. Jaw and W. R. Mason, *Inorg. Chem.*, 1989, **28**, 4370; M. M. Savas and W. R. Mason, *Inorg. Chem.*, 1987, **26**, 301.
23 D. Li, H. Xiao, C.-M. Che, W.-C. Lo and S.-M. Peng, *J. Chem. Soc., Dalton Trans.*, 1993, 2929.
24 C.-M. Che, V. W.-W. Yam, W.-T. Wong and T.-F. Lai, *Inorg. Chem.*, 1989, **28**, 2908; H.-K. Yip, C.-M. Che, Z.-Y. Zhou and T. C.-W. Mak, *J. Chem. Soc., Chem. Commun.*, 1992, 1369.

Received 6th July 1994; *Paper* 4/04117H